AIChE

Counter-Current Gas-Liquid Wavy Film Flow Between the Vertical Plates Analyzed Using the Navier-Stokes Equations

Yu. Ya. Trifonov
Institute of Thermophysics, Siberian Branch of Russian Academy of Sciences, Novosibirsk 630090, Russia

DOI 10.1002/aic.12128
Published online December 14, 2009 in Wiley InterScience (www.interscience.wiley.com).

The article is devoted to a theoretical analysis of counter-current gas-liquid wavy film flow between vertical plates. We consider two-dimensional nonlinear waves on the interface over a wide variation of parameters. The main interest is to analyse the wave structure at the parameter values corresponding to the onset of flooding observed in experiments. We use the Navier-Stokes equations in their full statement to describe the liquid phase hydrodynamics. For the gas phase equations, we use two models: (1) the Navier-Stokes system and (2) the simplified Benjamin-Miles approach where the liquid phase is a small disturbance for the laminar or turbulent gas flow. With the superficial gas velocity increasing and starting from some value of the velocity, the waves demonstrate a rapid decreasing of both the minimal film thickness and the phase wave velocity. We obtain a region of the gas velocity where we have two solutions at one set of the problem parameters and where the flooding takes place. Both the phase wave velocity and the minimal film thickness are positive numbers at such values of the velocity. We calculate the flooding point dependences on the liquid Reynolds number for two different liquids. The wave regime corresponding to the flooding point demonstrates negative u*-velocities in the neighbourhood of the interface near the film thickness maximum. At smaller values of the superficial gas velocity, the negative* u*-velocities take place in the neighbourhood of the film thickness minimum.* © 2009 American Institute of Chemical Engineers *AIChE J,* 56: 1975–1987, 2010
Keywords: viscous liquid film flow, nonlinear waves, counter-current gas liquid flow, flooding

Introduction

Theoretical studies of film flows began with the classical work of Nusselt,[1] where he obtained exact solutions of the Navier-Stokes equations for a thin viscous layer falling down a smooth vertical wall. The pioneering works of Kapitza[2] and Kapitza and Kapitza[3] followed this where they considered both experimentally and theoretically the different wavy flow regimes both in the presence and absence of interfacial shear. There are many theoretical and experimental papers devoted to the nonlinear waves on the surface of a free-falling liquid film (see, for example, Jones and Whitaker,[4] Chu and Dukler,[5] Alekseenko et al.,[6] Joo et al.,[7] Liu et al.,[8] Lee and Mei,[9] Chang and Demekhin,[10] Mudunuri and Balakotaiah,[11] Scheid et al.,[12]) where a complicated structure of the wavy film flow was revealed. We mention here some of the features (a) the existence of both spatial and temporal evolution of the film flow; (b) the transition of two-dimensional waves into three-dimensional structures; and (c) the existence of qualitatively different film flow regimes. Interfacial shear for a counter-current liquid-gas flow gives an additional interesting and technically important phenomenon—flooding. Semenov[13] was the first who observed this phenomenon experimentally. Thin layer of water falls down as a

Correspondence concerning this article should be addressed to Y. Y. Trifonov at trifonov@itp.nsc.ru.

film inside the glass vertical tube of $D = 8$, 13.8, and 22 mm in the experiments. The counter-current air velocity increases from 0 m/s to 35 m/s. He concluded that below the air velocity of 3–3.5 m/s (for tube of $D = 13.8$ mm), the gas flow had no effect on the liquid film wavy structure. Above the air velocity 4 m/s, the waves amplitude increased and at 7.3 m/s (for $D = 13.8$ mm), he observed flooding. A great number of works have been devoted to the prediction of the flooding for different liquids and gases and for different channels. There are many correlations in the literature to explain the flooding where the liquid changes direction (see, for example, the reviews by Dukler and Smith,[14] Tien and Liu,[15] and Drosos et al.,[16]). The general problem is that "the correlations are unable to predict flooding under conditions significantly different from the ones used to construct the correlations in the first place" (Maron and Dukler[17]). Most of the papers devoted to flooding are experimental measurements and observations. We mention here some of the experiments in vertical rectangular channels. Lee and Bankoff[18] conducted flooding experiments in a rectangular channel using steam-water counter-current flow. They indicated the significant effect of the channel gap on flooding. Biage et al.,[19] studied the case of air-water flow in a wide vertical channel with a relatively large gap. They showed that the onset of flooding is associated with droplet entrainment. Zapke and Kroeger[20,21] studied the dependence of flooding on duct-geometry and on gas/liquid physical properties (using several liquid and gas phases). Vlachos et al.,[22] reported flooding data obtained in a vertical rectangular channel with 5 and 10 mm gap. Sudo[23] carried out experiments in channels with gap and width 2.3 to 12.3 mm and 33 to 66 mm, respectively, and reported that the role of channel gap is very important. Drosos et al.,[16] reported data obtained in a vertical channel with 10 mm gap using air and three liquids (water, 1.5% and 2.5% aqueous butanol solutions). They presented results of visual observations, instantaneous local film thickness data, and shear stress data obtained by use of an electrochemical technique. The onset of flooding in their experiments was defined as "the condition where at least part of the liquid flow is reversed in direction and carried above the liquid entrance section, even in the form of droplets" (Hewitt[24]).

There are only a few theoretical works where the counter-current gas-liquid flow with a wavy interface is considered. Demekhin et al.,[25] using integral equations for the liquid phase, considered the gas turbulent flow as "pseudo-laminar" (Benjamin[26] and Miles[27]) to obtain the gas reaction to the liquid hydrodynamics. They computed the t-evolution of the initial x-periodical disturbances of the film thickness at different values of the nondimensional shear. At some value of the shear stress, they observed a dramatic increasing of the disturbance amplitude during the time evolution. The averaged film thickness is held constant in their calculations and the averaged liquid flow rate varies during the time-evolution. Dietze et al.,[28] using the Navier-Stokes equations for both phases, investigated the backflow phenomenon in falling liquid films when there was a no-slipping condition on the interface.

The goal of this work is to study different steady-state traveling regimes of counter-current gas-liquid film flow using the full Navier-Stokes equations. To define the flooding onset quantitatively, we need to analyze the wave structure changes when the problem parameters will be close to the critical parameters measured experimentally. A theoretical model for the onset of flooding provides the capability to analyze the flooding dependence on different geometrical parameters and on liquid/gas physical properties. To the best of our knowledge, this work is a first attempt in the literature to predict the onset of flooding theoretically using fundamental equations and principles. Using of the Navier-Stokes equations allows us to analyze the internal wave structure. The averaged flow rates for both phases are held constant in present calculations of nonlinear waves. It allows us to compare our calculations with experimental data. The onset of flooding is a limiting factor in the operation of various types of devices used by the chemical industry (for example, two-phase plate heat exchangers and compact reflux condensers). The flooding prediction will be interesting for many applications.

Governing Equations

Using a rectangular coordinate system, the Navier-Stokes equations with the corresponding boundary conditions describe the counter-current gas-liquid wavy film flow between vertical plates (see Figure 1):

$$\frac{\partial u}{\partial t} + u\frac{\partial u}{\partial x} + v\frac{\partial u}{\partial y} = -\frac{\partial P}{\partial x} + \frac{1}{\varepsilon \mathrm{Re}}\left(3 + \frac{\partial^2 u}{\partial y^2} + \varepsilon^2 \frac{\partial^2 u}{\partial x^2}\right); \quad (1)$$

$$\varepsilon^2\left(\frac{\partial v}{\partial t} + u\frac{\partial v}{\partial x} + v\frac{\partial v}{\partial y}\right) = -\frac{\partial P}{\partial y} + \frac{\varepsilon}{\mathrm{Re}}\left(\frac{\partial^2 v}{\partial y^2} + \varepsilon^2 \frac{\partial^2 v}{\partial x^2}\right);$$

$$\frac{\partial u}{\partial x} + \frac{\partial v}{\partial y} = 0; \quad (2,3)$$

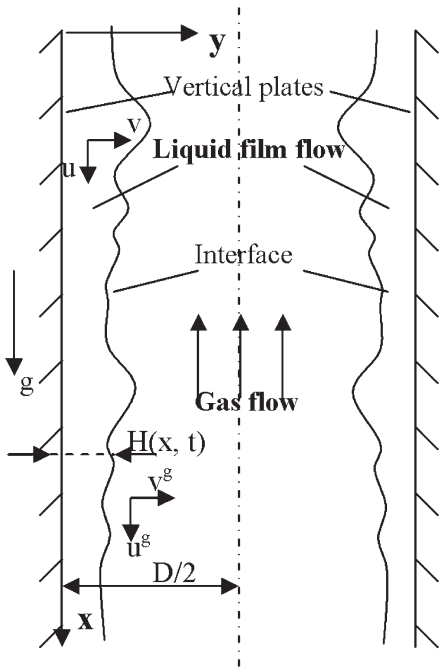

Figure 1. Scheme of counter-current gas/liquid flow.

$$u = v = 0, \quad y = 0; \quad v = \frac{\partial H}{\partial t} + u\frac{\partial H}{\partial x}, \quad y = H(x,t); \tag{4,5}$$

$$\left(\sigma_{ik}^g - \sigma_{ik}\right) n_k \tau_i = 0 \Rightarrow \varepsilon_\mu n \times \left(\frac{\partial u^g}{\partial y} + \varepsilon^2 \frac{\partial v^g}{\partial x} + 4\varepsilon^2 \frac{\partial v^g}{\partial y}\frac{\partial H}{\partial x}\frac{1}{1-\varepsilon^2\left(\frac{\partial H}{\partial x}\right)^2}\right) - \frac{\partial u}{\partial y} - \varepsilon^2 \frac{\partial v}{\partial x} - 4\varepsilon^2 \frac{\partial v}{\partial y}\frac{\partial H}{\partial x}\frac{1}{1-\varepsilon^2\left(\frac{\partial H}{\partial x}\right)^2} = 0, \qquad y = H(x,t); \tag{6}$$

$$\left(\sigma_{ik}^g - \sigma_{ik}\right) n_k n_i - \frac{\sigma}{R} = 0 \Rightarrow -\varepsilon_\rho n^2 P^g + P - \frac{2\varepsilon}{\mathrm{Re}}\left(\frac{\partial v}{\partial y} - \varepsilon_\mu n \frac{\partial v^g}{\partial y}\right)\frac{1+\varepsilon^2\left(\frac{\partial H}{\partial x}\right)^2}{1-\varepsilon^2\left(\frac{\partial H}{\partial x}\right)^2} + \frac{(3Fi)^{1/3}}{\mathrm{Re}^{5/3}}\frac{\varepsilon^2\frac{\partial^2 H}{\partial x^2}}{\left[1+\varepsilon^2\left(\frac{\partial H}{\partial x}\right)^2\right]^{3/2}} = 0, \qquad y = H(x,t); \tag{7}$$

$$u = nu^g, \quad v = nv^g, \quad y = H(x,t) \tag{8}$$

$$\frac{1}{n}\frac{\partial u^g}{\partial t} + u^g\frac{\partial u^g}{\partial x} + v^g\frac{\partial u^g}{\partial y} = -\frac{\partial P^g}{\partial x} + \frac{1}{\varepsilon\varepsilon_2 \mathrm{Re}^g}\left(\frac{\partial^2 u^g}{\partial y^2} + \varepsilon^2\frac{\partial^2 u^g}{\partial x^2}\right); \tag{9}$$

$$\varepsilon^2\left(\frac{1}{n}\frac{\partial v^g}{\partial t} + u^g\frac{\partial v^g}{\partial x} + v^g\frac{\partial v^g}{\partial y}\right) = -\frac{\partial P^g}{\partial y} + \frac{\varepsilon}{\varepsilon_2 \mathrm{Re}^g}\left(\frac{\partial^2 v^g}{\partial y^2} + \varepsilon^2\frac{\partial^2 v^g}{\partial x^2}\right); \tag{10}$$

$$\frac{\partial u^g}{\partial x} + \frac{\partial v^g}{\partial y} = 0; \quad \frac{\partial u^g}{\partial y} = 0, \quad v^g = 0, \quad y = \frac{1}{2\varepsilon_2} \tag{11,12}$$

Here, u is the liquid velocity component in the gravity direction, v is the liquid velocity in the y-direction, P is the pressure in the liquid, and σ_{ik} is the stress tensor components in liquid. The instantaneous local film thickness $H(x,t)$ is the interface shape and (u^g,v^g) are the gas velocity components in the x- and y-directions, respectively. Pressure in the gas is P^g, σ_{ik}^g is the stress tensor components in gas, $\boldsymbol{n_k}$ and τ_i are the components of normal and tangential unit vectors to the interface, respectively. The interface curvature radius is R and we assume summing over repeated indexes in the boundary conditions.

There is symmetry of the two-phase flow with respect to the channel middle (see Figure 1). It is enough to consider the equations for $0 \le y \le 0.5/\varepsilon_2$ and Eq. 12 is the symmetry condition. Equations 1, 2, 9, and 10 represent momentum conservation for the liquid and gas phase, respectively. Equations 3 and 11 is the mass conservation law for the liquid and gas, correspondingly. Equations 4 and 8 are the no-slip conditions on the plate and on the interface, respectively. Equation 5 is a kinematic condition along the interface. Equations 6 and 7 formulate the tangential and normal stress equilibrium along the interface, correspondingly.

Equations 1–12 are in a nondimensional form and we used scales as follows (asterisk denotes the dimensional variables):

$$x = \frac{x*}{L}; t = \frac{u_0 t*}{L}; y = \frac{y*}{H_0}; u = \frac{u*}{u_0}; v = \frac{v*}{\varepsilon u_0}; P = \frac{P*}{\rho u_0^2};$$

$$H = \frac{H*}{H_0}; u^g = \frac{(u^g)*}{u_0^g}; v^g = \frac{(v^g)*}{\varepsilon u_0^g}; P^g = \frac{(P^g)*}{\rho_g (u_0^g)^2};$$

$$\mathrm{Re} = \frac{u_0 H_0}{\nu} = \frac{g(1-\varepsilon_\rho)H_0^3}{3\nu^2}; \varepsilon = \frac{H_0}{L}; \varepsilon_2 = \frac{H_0}{D};$$

$$\varepsilon_\mu = \frac{\mu_g}{\mu}; \varepsilon_\rho = \frac{\rho_g}{\rho}; n = \frac{u_0^g}{u_0}; \mathrm{Re}^g = \frac{u_0^g D}{\nu_g}; Fi = \frac{(\sigma/\rho)^3}{g(1-\varepsilon_\rho)\nu^4}.$$

Here, ν, μ is the liquid kinematic and dynamic viscosity, respectively, ρ is the liquid density, σ is the surface tension. The wave period is L, Re is the liquid Reynolds number and Fi is the film number. The gas kinematic and dynamic viscosities are ν_g, μ_g, respectively, ρ_g is the liquid density, Re^g is the gas Reynolds number, u_0^g is a half of the gas superficial velocity U_{GS} ($u_0^g = 0.5U_{GS} = 0.5Q_G/S$, Q_G is the volumetric gas flow rate supplied per the channel cross-section $S = wD$, w is the channel width, D is the distance between the vertical plates).

The free surface shape is unknown beforehand. Further, we consider the steady-state travelling solutions of the Eqs. 1–12, $[H(x - ct), u(x - ct,y), v(x - ct,y), Z\varepsilon_\rho n^2 x + \bar{P}(x - ct, y), u^g(x - ct, y), v^g(x - ct, y), \mathrm{Z}x + \bar{P}^g(x - ct, y)]$, $\boldsymbol{c}$ is the wave phase velocity and Z = const. Values of both $\boldsymbol{c}$ and Z are unknown beforehand. The coordinates transformation $x_1 = x - ct$, $\eta = y/H$, $\tilde{\eta} = (0.5 - \varepsilon_2 y)/(0.5 - \varepsilon_2 H)$ allows us to define the flow area: $x_1 \in [0,1]$, $\eta \in [0,1]$, $\tilde{\eta} \in [0,1]$. We use spectral method to obtain the steady-state solutions and Appendix A gives the numerical algorithm details.

There are eight parameters in the Eqs. 1–12, ε, ε_2, ε_μ, ε_ρ, n, Fi, Re, Re^g. It is easy to see that $n = \frac{\varepsilon_2\varepsilon_\mu}{\varepsilon_\rho}\frac{\mathrm{Re}^g}{\mathrm{Re}}$ and only seven parameters are independent. We will use $\lambda_{neut}/L, \mathrm{Ka}, \mathrm{Re}, \sqrt{\sigma/\rho g(1-\varepsilon_\rho)}/D, \varepsilon_\mu, \varepsilon_\rho, \mathrm{Re}^g$ as the independent parameters for the calculations below, where λ_{neut} is the wavelength of the neutral disturbance of the wavyless solution and $\mathrm{Ka} \equiv Fi^{1/11}$, Ka is the Kapitsa number. It is evident that $\lambda_{neut} = H_0 f(\mathrm{Ka}, \mathrm{Re}, \sqrt{\sigma/\rho g(1-\varepsilon_\rho)}/D, \varepsilon_\mu, \varepsilon_\rho, \mathrm{Re}^g)$ and the equations parameters may be defined using our independent parameters, $\varepsilon_2 = (3\mathrm{Re}/\mathrm{Ka})^{1/3}\left(\sqrt{\sigma/\rho g(1-\varepsilon_\rho)}/D\right)/\mathrm{Ka}^{3/2}$, $\varepsilon = (H_0/\lambda_{neut})(\lambda_{neut}/L)$.

Our choice of the independent parameters set has several advantages. Values of the parameters Ka, $\sqrt{\sigma/\rho g(1-\varepsilon_\rho)}/D, \varepsilon_\mu, \varepsilon_\rho$ depend only on the liquid/gas physical properties and on the gas channel geometry. Only values of the parameters Re and Re^g vary with the liquid/gas flow rate changing. Choice of the value λ_{neut}/L as the independent parameter allows us to compare the results of the Navier-Stokes calculations with the predictions of different integral and asymptotic approaches where the value of the neutral wavelength is different.

Let us draw attention that both the averaged liquid flow rate and the averaged gas flow rate are held constant in our calculations. Taking into account the kinematic condition (5), the no-slip conditions (4), (8) and the symmetry condition (12) the integration of the continuity Eqs. 3 and 11 gives

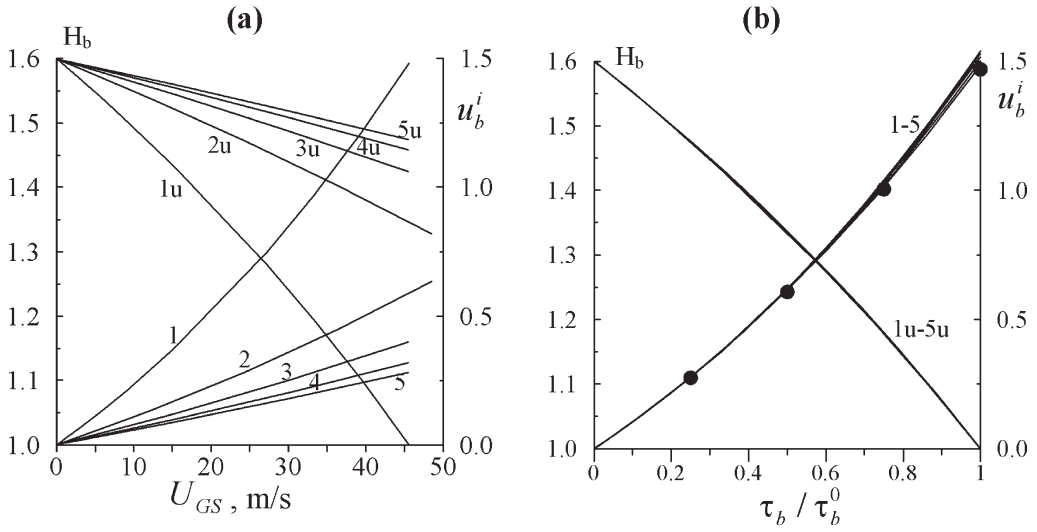

Figure 2. The basic solution with smooth interface.

Film thickness (lines 1–5) and liquid interface velocity (lines 1u-5u) variations with the gas superficial velocity (a) and with non-dimensional interfacial shear (b). Lines 1–5 and 1u-5u were computed at Re = 1, 10, 30, 60 and 90, respectively. Symbols correspond to the "basic" solution calculations by Maron and Dukler.[17]

$$q(x_1) - cH(x_1) = const = \langle q \rangle - c\langle H \rangle = 1 - c\langle H \rangle,$$

$$q \equiv \int_0^H udy; q^g(x_1) + \frac{cH(x_1)}{n} = const = \langle q^g \rangle + \frac{c}{n}\langle H \rangle$$

$$= -\frac{1}{\varepsilon_2} + \frac{c}{n}\langle H \rangle,\ q^g \equiv \int_H^{0.5/\varepsilon_2} u^g dy.$$

Here $\langle \ldots \rangle$ is the value averaged over a wavelength. Value of $\langle q^g \rangle$ is negative because we consider a counter-current gas/liquid flow. Using variables η and $\tilde{\eta}$, we obtain Eqs. A4 and A10. The constant-flux formulation corresponds to the experimental situation. This formulation is much closer to the reality where the mass conservation takes place during a spatial-temporal evolution.

Results of the Calculations

The current calculations are primarily based on the air/water system and one value of the spacing between the plates $D = 10$ mm. These conditions correspond to Drosos et al.,[16] experiments. Drosos et al.,[16] measured the onset of flooding for the air/water system around 8–12 m/s, depending on the value of Re. They obtained that the superficial gas velocity at the onset of flooding decreases with the liquid Reynolds number increasing. Our goal is to predict theoretically these numbers of the flooding onset and its dependence on Re using the fundamental equations and principles. We will vary the liquid Reynolds number, wavelength and the gas Reynolds number to see what happening with the steady-state travelling solutions when the parameters are close to the experimental flooding condition.

As a first step, we compute the main characteristics of the "basic" wavyless solution. Figure 2 demonstrates these results. With increasing in the superficial gas velocity U_{GS}, the velocity at the interface approaches zero and this state was called by Maron and Dukler[17] as the "O" state (τ_b^0 denotes the interfacial shear at this state in Figure 2). The value of U_{GS}, corresponding to the "O" state in Figure 2, is much higher in comparison to the superficial gas velocity measured experimentally at the flooding condition. For example, value of this velocity is close to 45 m/s at Re = 1 (intersection of line 1u with the x-axis in Figure 2) and increases dramatically with the increasing in Re, unlike the experimental results of the flooding onset described above in this section. We need to involve wavy interface to analyze the liquid/gas interaction more correctly.

Figure 3 demonstrates the main characteristics of the nonlinear steady-state solutions of very small amplitude (α_{neut}

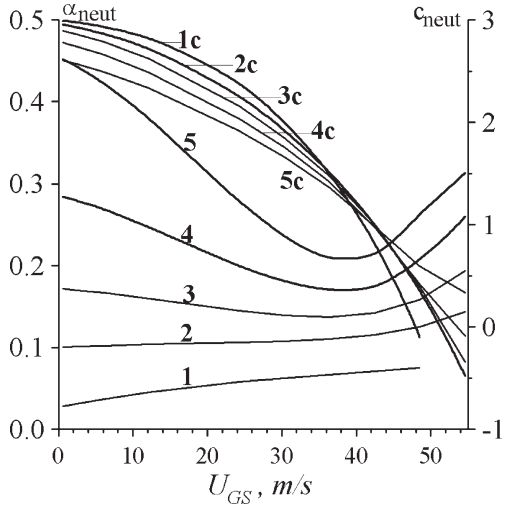

Figure 3. Wave number (lines 1–5) and phase velocity (lines 1c–5c) of neutral disturbances as a function of gas superficial velocity.

Lines 1–5 were computed at Re = 1, 5, 10, 20 and 40, respectively.

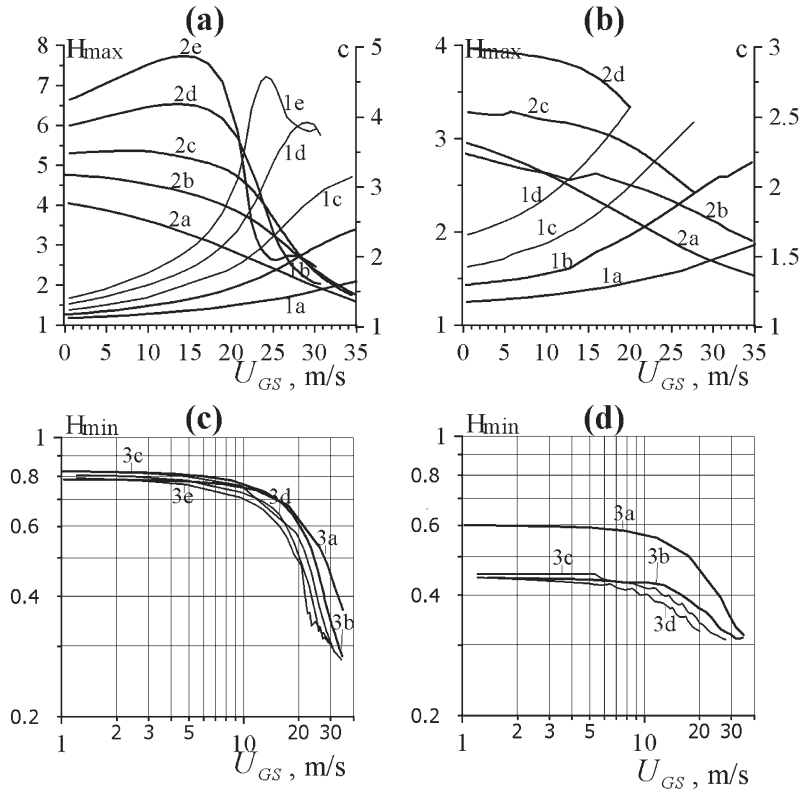

Figure 4. Maximal (lines 1a–1e) and minimal (lines 3a–3e) values of wavy film thickness, and phase velocity (lines 2a–2e) of nonlinear wavy regimes as a function of gas superficial velocity computed at different values of wavelength (a, λ_{neut}/L = 0.8; b, 0.4; c, 0.25; d, 0.15; e, 0.1).

Figures (a) and (c) correspond to Re = 5; (b) and (d), 20.

$\equiv 2\pi/\lambda_{neut}$). Such solutions are close to neutral disturbances of the linear-stability problem of the wavyless solution. Amplitude of the first harmonic of the film-thickness Fourier expansion is a small constant value in the computations of such solutions (for example, $\mathrm{Im}(H^1) = 10^{-5}$). The wavelength λ_{neut} is unknown instead of the $\mathrm{Im}(H^1)$ during the numerical computations of Eqs. 1–12. Wave number of the neutral disturbance monotonically increases with increasing U_{GS} at small values of Re, as it shown in Figure 3. The dependence has local minimum at large values of Re (see Figure 3). Results presented in Figure 3 are in good agreement with the computations of Demekhin et al.,[25] where they investigated the linear stability of the wavyless solution using the "quasi-laminar" assumption for the turbulent gas flow. Phase velocity c_{neut} of the neutral disturbances decreases with increasing superficial gas velocity U_{GS} and becomes negative at $U_{GS} > U^*_{GS}$ (Re), as it presented in Figure 3. The critical values U^*_{GS} (Re) are closer to the corresponding experimental values[16] of the flooding onset in comparison to the values of the "O" state discussed above, but the difference between the prediction and experiment is still large. The values of U^*_{GS} are around 50 m/s in Figure 3 and the onset of flooding in experiments is around 10 m/s. With increases in Re, the value of U^*_{GS} increases and we have the same contradiction with the flooding onset experiments as for the "O" state. Computations of the weakly nonlinear solutions do not predict the flooding onset and we need to analyse the nonlinear waves far from the linear stability curve.

Varying the values of (λ_{neut}/L, Re, Re^g), we compute the steady-state travelling regimes of Eqs. 1–12 over a wide range of the independent parameters. We present these results in Figures 4–6. At small values of U_{GS}, the nonlinear solutions are close to the waves on the surface of a liquid film falling down under an action of gravity (see paper by Trifonov[29]). In the case of gravity flow, a wave which branched from the basic solution exists for $\lambda_{neut}/L \leq 1$. At small Re, the "long wave" looks like a succession of "solitary humps", unlike the case of large values of Re where the "long wave" looks like a succession of "solitary dips". In the case of gravity flow, there are several nonlinear solutions for a fixed set of the independent parameters at moderate values of Re and for $\lambda_{neut}/L \leq 0.4 \div 0.5$.[29] Each of the solutions has continuation into the region of "long" waves and the number of such solutions increases with decreasing λ_{neut}/L. We found here that the interfacial shear simplifies the "general picture of the nonlinear solutions". At moderate values of U_{GS}, the "long wave" looks like a succession of "solitary humps" at all values of Re. In Figure 4 we present the maximal and minimal values of the film thickness and the phase velocity of the nonlinear waves at λ_{neut}/L = 0.1, 0.15, 0.25, 0.4 and 0.8. We use a continuation method to obtain these dependences. As a first step, we compute the

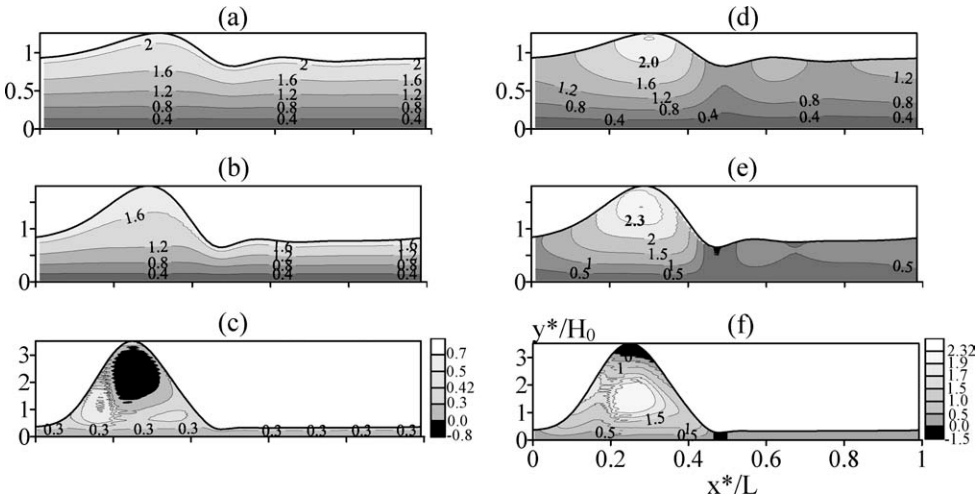

Figure 5. Contour lines of the streamline function (a–c) in a reference frame that moves with the wave phase velocity (in this coordinate system the liquid particle moves along the contour lines) and the contour lines of the u-velocity (d–f).

Here, Re = 5 and $\lambda_{neut}/L = 0.4$; (a), (d) correspond to $U_{GS} = 0.3$ m/s; (b) and (e), U_{GS} =18 m/s; (c) and (f), $U_{GS} = 35$ m/s.

waves branched from the "basic" wavyless solution for wide range of $0.1 \leq \lambda_{neut}/L \leq 1$. We do these computations for two values of the liquid Reynolds number Re = 5, 20 at constant value of the superficial gas velocity $U_{GS} = 10[m/s]$. As a second step, we vary the value of U_{GS} at constant values of λ_{neut}/L and Re to obtain the dependences in Figure 4. In Figures 5 and 6, we present the wavy profiles of the solution film thickness and the contour lines of both the streamline function $\Psi(\boldsymbol{x}, \eta) = \int_0^{\eta} (\boldsymbol{c} - \boldsymbol{u})\boldsymbol{H}\boldsymbol{d}\eta'$ (in a moving coordinate system) and the $u(x, \eta)$ component velocity (in a laboratory coordinate system). In a coordinate system moving with the solution phase velocity, the liquid particle trajectory coincides with the contour lines. Figure 5 corresponds to Re = 5 and Figure 6, Re = 20.

With increasing superficial gas velocity, the wave amplitude increases as shown in Figures. 4–6. The wave velocity and the minimal film thickness decreases with increasing U_{GS}. Essential changes in H_{max}, H_{min} and c start from some value of $U_{GS} \approx 10$ [m/s], as shown in Figure 4. The computed solutions demonstrate an internal vortex at large value of G_{GS}. The u-velocity distribution in Figures 5 and 6 demonstrates a region of flow reversal near the film thickness minimum. At large values of U_{GS}, negative u-velocities exist

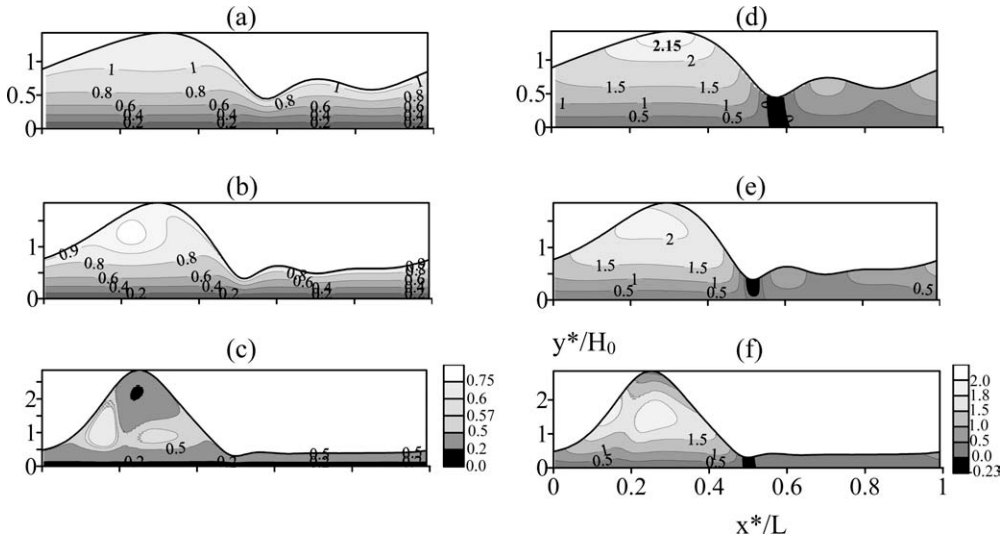

Figure 6. Contour lines of the streamline function (a–c) in a reference frame that moves with the wave phase velocity (in this coordinate system the liquid particle moves along the contour lines) and the contour lines of the u-velocity (d–f).

Here, Re = 20 and $\lambda_{neut}/L = 0.4$; (a) and (d) correspond to $U_{GS} = 0.3$ m/s; (b) and (e), $U_{GS} = 18$ m/s; (c) and (f), $U_{GS} = 35$ m/s.

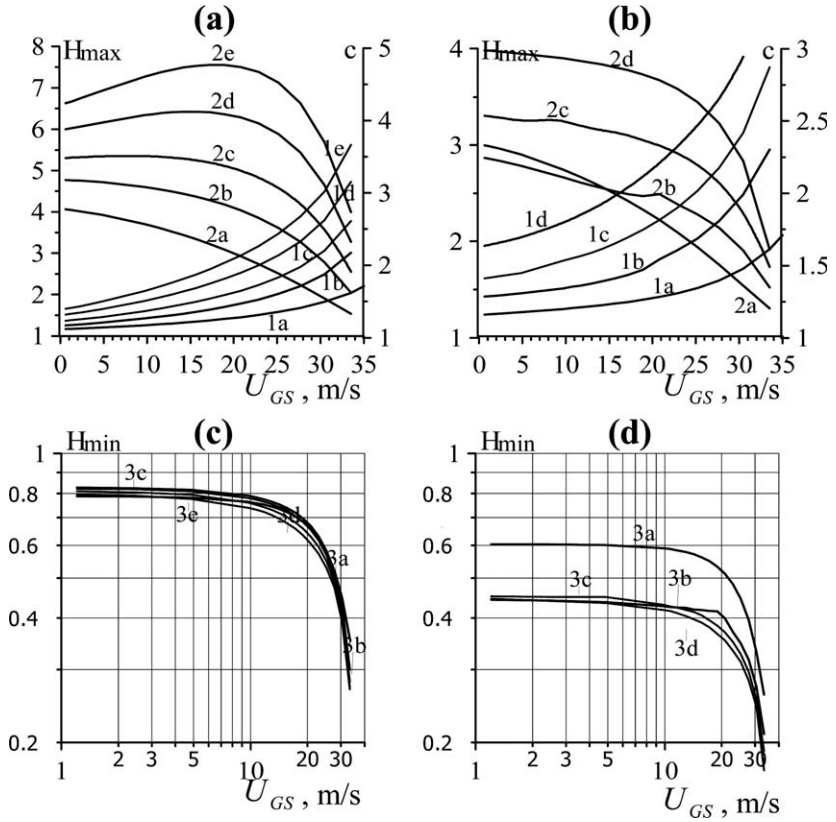

Figure 7. These calculations use a simplified approach[13–20] with the laminar velocity profile to obtain the gas reaction.

Maximal (lines 1a–1e) and minimal (lines 3a–3e) values of wavy film thickness, and phase velocity (lines 2a–2e) of nonlinear wavy regimes as a function of gas superficial velocity computed at different values of wavelength (a, $\lambda_{neut}/L = 0.8$; b, 0.4; c, 0.25; d, 0.15; e, 0.1). Figures (a, c) correspond to Re = 5; (b, d), 20.

near the film thickness maximum (see Figure 5). Malamataris et al.,[30] computations of the Navier-Stokes equations corresponding to the gravity flow of liquid films demonstrate flow reversal only near the film thickness minimum.

Results of the nonlinear wave computations presented in Figures 3–6 allow us to conclude that there is an essential disagreement between the prediction and the Drosos et al.,[16] measurement of the flooding onset. Calculations based on the Navier-Stokes equations for both phases give us very large values of superficial gas velocity where the solution transformation looks like the corresponding changes at the onset of flooding in experiments. One of the main reasons is that the gas flow in our calculations suggests an eddy laminar flow. In reality, the gas flow is turbulent at the values of the gas velocity corresponding to the onset of flooding. For example, the value of the superficial gas velocity $U_{GS} =$ 9 m/s in the case of air corresponds to the twelve thousands of the gas Reynolds number that based on the channel hydraulic diameter. It was not evident beforehand that the eddy gas flow with a large number of the Chebyshev polynomials considered in the paper will give us so big value of U_{GS} corresponding to the onset of flooding. Our approach assumes that the complicated gas phase solution [u^g (t,x,y), v^g (t,x,y), P^g (t,x,y)] has a form of the steady-state travelling wave [u^g ($x - ct$,y), v^g ($x - ct$,y), P^g ($x - ct$,y)]. This is a possible reason of the rough approximation of real flow where the continuous generation and disappearing of eddies of different scales takes place at such value of Re^g.

Simplified equations of the reaction of the laminar or turbulent gas on the wavy liquid film

Miles[27] and Benjamin[26] were the first who considered the liquid wavy film flow as a small disturbance for the turbulent or laminar gas flow between the plates. In this case, the gas velocities and pressure have form $u^g = u_b^g + \hat{u}^g$, $v^g = \hat{v}^g$, $P^g = P_b^g + \hat{P}^g$ where the $u_b^g(y)$, $P_b^g(x)$ correspond to a basic solution of the laminar or turbulent gas flow through a smooth channel and the values $\hat{u}^g(x,y), \hat{v}^g(x,y), \hat{P}^g(x,y)$ correspond to the gas flow perturbations due to the thin liquid film falling down the channel wall. Linearization of the governing equations (see Eqs. 8–12 for the laminar flow) near the basic solution gives

$$\hat{u}^g + \frac{du_b^g}{dy} H(x) = 0,\ \hat{v}^g = 0, y = 0 \tag{13}$$

$$u_b^g \frac{\partial \hat{u}^g}{\partial x} + \hat{v}^g \frac{du_b^g}{dy} = -\frac{\partial \hat{P}^g}{\partial x} + \frac{1}{\varepsilon\varepsilon_2 \mathrm{Re}^g}\left(\frac{\partial^2 \hat{u}^g}{\partial y^2} + \varepsilon^2 \frac{\partial^2 \hat{u}^g}{\partial x^2}\right); \tag{14}$$

$$\varepsilon^2 u_b^g \frac{\partial \hat{v}^g}{\partial x} = -\frac{\partial \hat{P}^g}{\partial y} + \frac{\varepsilon}{\varepsilon_2 \mathrm{Re}^g}\left(\frac{\partial^2 \hat{v}^g}{\partial y^2} + \varepsilon^2 \frac{\partial^2 \hat{v}^g}{\partial x^2}\right); \tag{15}$$

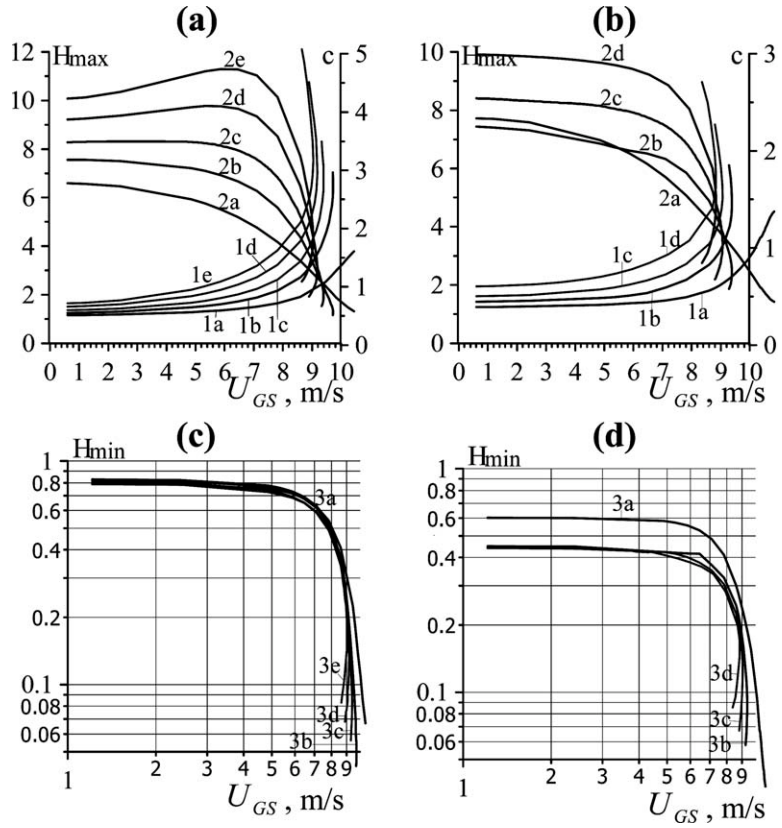

Figure 8. These calculations use a simplified approach (13–20)) with the turbulent velocity profile to obtain the gas reaction.

Maximal (lines 1a–1e) and minimal (lines 3a–3e) values of wavy film thickness, and phase velocity (lines 2a–2e) of nonlinear wavy regimes as a function of gas superficial velocity computed at different values of wavelength (a, $\lambda_{neut}/L = 0.8$; b, 0.4; c, 0.25; d, 0.15; e, 0.1). Figures (a, c) correspond to Re = 5; (b, d), 20.

$$\frac{\partial \hat{u}^g}{\partial x}+\frac{\partial \hat{v}^g}{\partial y}=0; \quad \frac{\partial \hat{u}^g}{\partial y}=0, \hat{v}^g=0, \; y=\frac{1}{2\varepsilon_2} \qquad (16,17)$$

We neglect terms c/n, u/n and v/n (at the flooding conditions the gas superficial velocity is much higher than the liquid film velocity, $n \gg 1$) and present the no-slip conditions along the interface using an expansion of the gas velocities near the wall.

Let us emphasize that the Eqs. 13–17 are valid both for laminar and turbulent gas flow. In the case of turbulent flow, we use the mean-velocity profiles $u_b^g(y), P_b^g(x), \hat{u}^g(x,y)$, $\hat{v}^g(x,y), \hat{P}^g(x,y)$. The pulsations terms of the linearized equations are negligible.

We solve Eqs. 13–17 independently from the governing equations of the liquid film flow (see Appendix B for details). This is a linear system where the Fourier harmonic H^k of the film thickness $H(x)$ generates the corresponding gas reaction (F^k (y), $P_g^k(y)$. Taking into account Eq. 16, the perturbation fields $\hat{u}^g, \hat{v}^g, \hat{P}^g$ are as follows:

$$\hat{u}^g(x,y)=-\sum_{k=-N/2+1}^{N/2-1}\frac{dF^k}{dy}H^k\exp(2\pi ikx), \left(F^{-k}\right)^*=F^k; \quad (18)$$

$$\hat{v}^g(x,y)=\sum_{k=-N/2+1}^{N/2-1}2\pi ikF^k(y)H^k\exp(2\pi ikx); \qquad (19)$$

$$\hat{P}^g(x,y)=\sum_{k=-N/2+1}^{N/2-1}P_g^k(y)H^k\exp(2\pi ikx), \left(P_g^{-k}\right)^*=P_g^k. \quad (20)$$

Thus, we reduce the two-phase problem to the solving of the liquid film flow Eqs. A1–A5 with the modified boundary conditions (B8), (B9). It is easy to see that $Z=\lambda^f \varepsilon_2/\varepsilon$ in the equations (see Appendix B) and λ^f is the friction coefficient for the gas flow between the smooth plates. We use spectral method to compute the steady-state solutions of these equations.

Figure 7 demonstrates results where the undisturbed gas velocity in Eqs. 13–17 has a laminar profile (B4). These results are close to the corresponding computations in Figure 4 where the Navier-Stokes equations used for both phases. The comparison allows us to conclude that the simplified approach works well for the flooding calculations.

Figures 8–11 show results of the computations where the undisturbed gas velocity in Eqs. 13–17 has a turbulent profile (B5). These calculations agree with the experimental measurements and observations of the flooding onset. At relatively small values of the gas superficial velocity $U_{GS} \leq 10$ [m/s], we can see the ''large'' waves moving over a thin sublayer (see Figures. 9d,h and 10d,h). Amplitude of the ''large'' waves is several times bigger than the wave amplitude of a freely down liquid film (see Figures 8, 9, and 10 at small values of U_{GS}). Qualitatively, the solutions

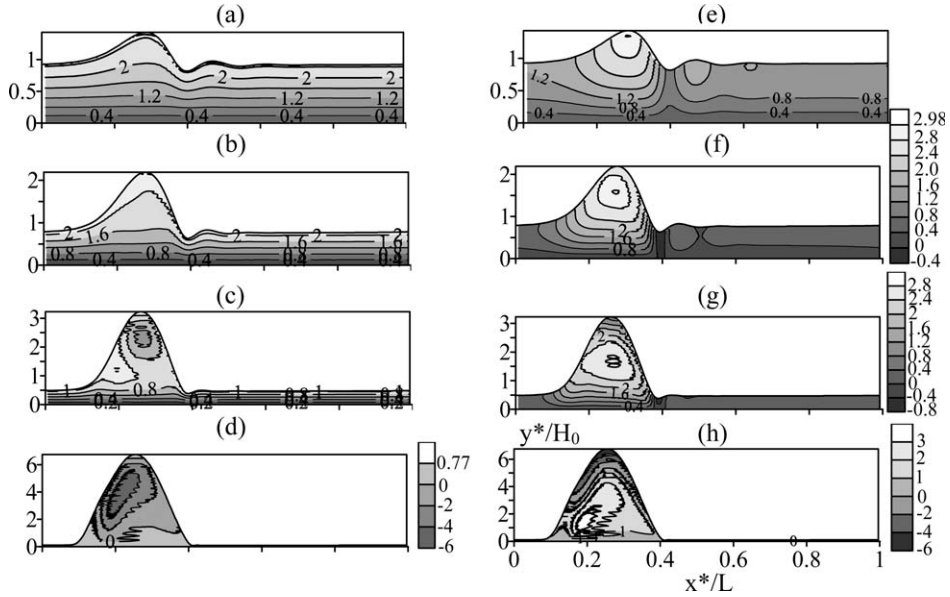

Figure 9. Contour lines of the streamline function (a–d) in a reference frame that moves with the wave phase velocity (in this coordinate system the liquid particle moves along the contour lines) and the contour lines of the u-velocity (e–h).

Here, Re = 5 and $\lambda_{neut}/L = 0.25$; (a) and (e) correspond to $U_{GS} = 2.5$ m/s; (b) and (f), $U_{GS} = 7.0$ m/s; (c) and (g), $U_{GS} = 8.5$ m/s; (d) and (h), $U_{GS} = 9.4$ m/s.

transformation with the U_{GS} increasing looks alike at all values of the wavelength considered in the paper (except the short waves with $\lambda_{neut}/L = 0.8$). With the wavelength increasing, the distance between the "large" waves increases. The sublayer thickness almost does not depend on the wavelength (see Figure 8).

At some values of U_{GS}, the calculations demonstrate the negative *u*-velocities around the film thickness maximum (Figure 9h and Figure 10h). We found that such values of U_{GS} correspond to the small neighbourhood of the "returning" point (U^f_{GS}) of the dependences in Figure 8 where the derivatives dH_{max}/dU_{GS}, dc/dU_{GS} and dH_{min}/dU_{GS} change sign. We did not obtain solutions at $U_{GS} > U^f_{GS}$ and this is why we call the point (U^f_{GS}) as the "returning" point. There are two solutions in a small neighbourhood of the "returning" point at one value of the superficial gas velocity. We

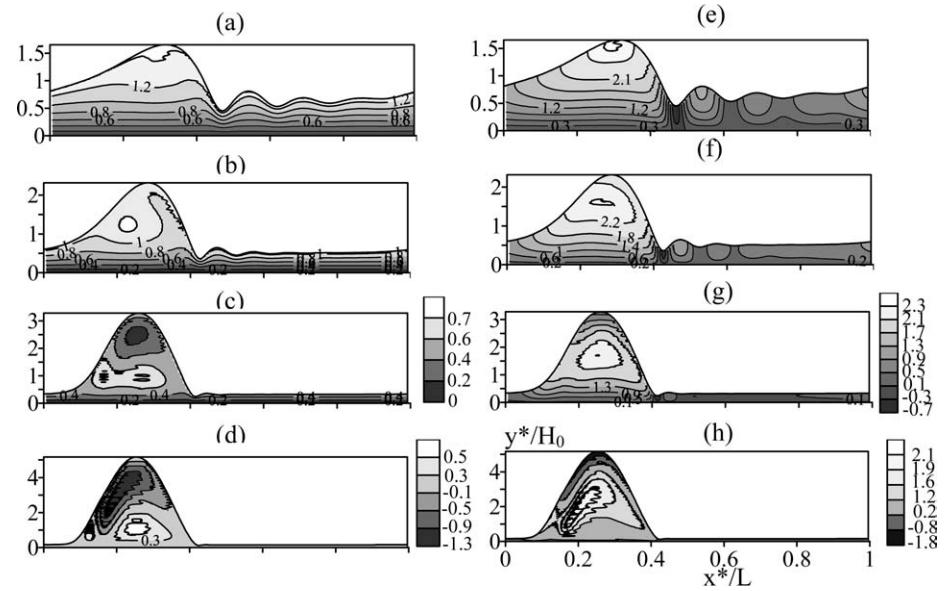

Figure 10. Contour lines of the streamline function (a–d) in a reference frame that moves with the wave phase velocity (in this coordinate system the liquid particle moves along the contour lines) and the contour lines of the u-velocity (e–h).

Here, Re = 20 and $\lambda_{neut}/L = 0.25$; (a) and (e) correspond to $U_{GS} = 2.5$ m/s; (b) and (f), $U_{GS} = 7.0$ m/s; (c) and (g) $U_{GS} = 8.5$ m/s; (d) and (h) $U_{GS} = 9.07$ m/s.

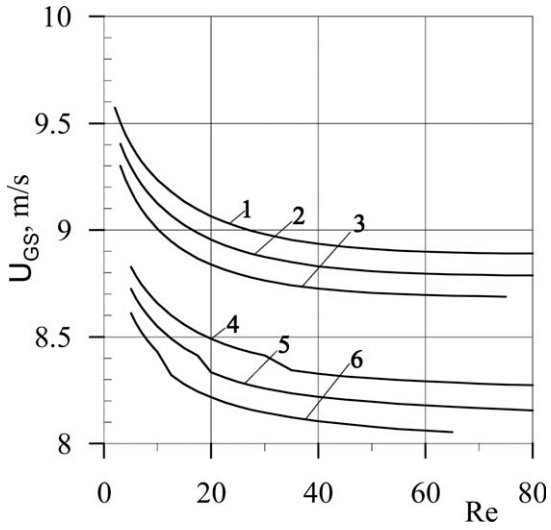

Figure 11. Superficial gas velocity, U_{GS}, corresponding to the "onset of flooding" vs. Re for two liquids.

Lines 1–3 correspond to water at $\lambda_{neut}/L = 0.25, 0.2, 0.15$, respectively. Lines 4–6 correspond to 2.5% butanol at $\lambda_{neut}/L = 0.25, 0.2, 0.15$, respectively.

obtain the "returning" points for all values of the wavelength and the liquid Reynolds number considered in the paper (except the short waves with $\lambda_{neut}/L = 0.8$). With the λ_{neut}/L decreasing, the dependence of U^f_{GS} on the wavelength is not strong and we can define the flooding velocity as a value of U^f_{GS} for the long waves.

Figure 11 shows results of the computations of the flooding velocity U^f_{GS} (Re)for two different liquids. We compute the flooding curves for three values of the wavelength. In accordance with the nondimensional parameters of our equations, the flooding curve is a function of six variables and has the form as follows:

$$\mathrm{Re}^{gf} = \mathrm{Re}^{gf}(\lambda_{neut}/L, \mathrm{Ka}, \mathrm{Re}, \sqrt{\sigma/\rho g(1-\varepsilon_\rho)}/D, \varepsilon_\mu, \varepsilon_\rho)$$

The developed approach allows us to compute the flooding curves at variation of different parameters. For example, we can analyze the influence of the distance between the plates on the flooding and obtain the curves $\mathrm{Re}^{gf}(\sqrt{\sigma/\rho g(1-\varepsilon_\rho)}/D)$ at constant values of the parameters $\lambda_{neut}/L, \mathrm{Ka}, \mathrm{Re}, \varepsilon_\mu, \varepsilon_\rho$. The systematic computation of the flooding curves is a goal of a separate investigation due to amount of the independent parameters

Conclusions

We considered the counter-current wavy gas/liquid film flow between vertical plates. We used the Navier-Stokes equations in their full statement to describe liquid phase hydrodynamics. For the gas phase equations, we used two models: (1) the Navier-Stokes system and (2) the simplified Benjamin-Miles approach where the liquid phase is a small disturbance for the laminar or turbulent gas flow. Our goal was to predict theoretically flooding onset using the fundamental equations and principles. We varied the liquid Reynolds number, wavelength and the gas Reynolds number to see what happening with the steady-state travelling solutions when the parameters were close to the experimental flooding condition.

We obtained that there were seven independent parameters to describe the gas/liquid wavy dynamics $\lambda_{neut}/L, \mathrm{Ka}, \mathrm{Re}, \mathrm{Re}^g, \sqrt{\sigma/\rho g(1-\varepsilon_\rho)}/D, \varepsilon_\mu, \varepsilon_\rho$, λ_{neut} is a dimensional wavelength of the neutral disturbance of the smooth solution, L is a spatial period of the nonlinear regime, $\mathrm{Ka} = ((\sigma/\rho)^3/g(1-\varepsilon_\rho)\nu^4)^{1/11}$ is the Kapitza's number, D is a distance between the plates, $\varepsilon_\mu = \mu_g/\mu$ and $\varepsilon_\rho = \rho_g/\rho$.

We found that with the superficial gas velocity increasing and starting from some value of the velocity, the waves demonstrate a rapid decrease of both the minimum film thickness and the phase wave velocity. At the same time, the maximum film thickness increases and finally the wave structure demonstrates the negative u-velocities in the neighbourhood of the maximum. Both the wave celerity and the film thickness minimum are still positive numbers at such values of the superficial gas velocity. The values of the film thickness maximum obtained in our computations were small for the channel bridging. The described transformation of the wave structure with the superficial gas velocity increasing takes place for both models of the gas hydrodynamics. Calculations based on the Navier-Stokes equations for both phases gave us very large values of the superficial gas velocity where the described transformation took place. We found that the computations based on the Navier-Stokes equations for the liquid phase and on the Benjamin-Miles approach with the turbulent profile for the gas phase demonstrate a reasonable agreement with the experimental observations and measurements of the flooding onset. We found a region of the "returning point" of the superficial velocity where we have several solutions and where the flooding takes place. We did not obtain the steady-state traveling solutions when the superficial gas velocity is greater than the value corresponding to the "returning" point. These findings allowed us to define the onset of flooding mathematically and to obtain its dependence on the liquid Reynolds number and on the liquid physical properties. The wave regime corresponding to the flooding point demonstrates negative u-velocities in the neighbourhood of the interface near the film thickness maximum. At smaller values of the superficial velocity, the negative u-velocities take place in the neighbourhood of the film thickness minimum.

Literature Cited

1. Nusselt W. Die oberflächenkondensation des wasserdampfes. *Z Ver Deut Ing*. 1916;60:541–546.
2. Kapitza PL. Wave flow of thin viscous liquid films. *Zh Teor Fiz*. 1948;18:3–28.
3. Kapitza PL, Kapitza SP. Wave flow of thin viscous liquid films. *Zh Teor Fiz*. 1949;19:105–120.
4. Jones LO, Whitaker S. An experimental study of falling liquid films. *AIChE J*. 1966;12:525–529.
5. Chu KI, Dukler AE. Statistical characteristics of thin wavy films. *AIChE J*. 1974;20:695–706.
6. Alekseenko SV, Nakoryakov VE, Pokusaev BG. Wave formation on a vertical falling liquid film. *AIChE J*. 1985;31:1446–1460.
7. Joo SW, Davis SH, Bankoff SG. Long-wave instabilities of heated falling films: two-dimensional theory of uniform layers. *J. Fluid Mech*. 1991;230:117.
8. Liu J, Paul JD, Gollub JP. Measurements of the primary instabilities of film flow. *J Fluid Mech*. 1993;250:69–101.

9. Lee JJ, Mei CC. Stationary waves on an inclined sheet of viscous fluid at high Reynolds and moderate Weber numbers. *J Fluid Mech.* 1996;307:191–229.
10. Chang HC, Demekhin EA. *Complex Wave Dynamics on Thin Films*. Amsterdam: Elsevier Science, 2002.
11. Mudunuri RR, Balakotaiah V. Solitary waves on thin falling films in the very low forcing frequency limit. *AIChE J*. 2006;52:3995–4003.
12. Scheid B, Ruyer-Quil C, Manneville P. Wave patterns in film flows: modeling and three-dimensional waves. *J Fluid Mech.* 2006;562: 183–222.
13. Semenov PA. The liquid flow of thin layers. *Zh Tehn Fiz.* 1944;14: 427–437.
14. Dukler AE, Smith L. Two phase interactions in countercurrent two phase flow: studies of the flooding mechanism. U.S. Nuclear Regulatory Comission Report, NUREG/CR-0617, 1977.
15. Tien CL, Liu CP. Studies on vertical two phase countercurrent flooding. Electric Power Research Institute Report, NP-984, 1979.
16. Drosos EIP, Paras SV, Karabelas AJ. Counter-current gas-liquid flow in a vertical narrow channel—liquid film characteristics and flooding phenomena. *Int J Multiphase Flow*. 2006;32:51–81.
17. Maron DM, Dukler AE. Flooding and upward film flow in vertical tubes. II. Speculations on film flow mechanisms. *Int J Multiphase Flow*. 1984;10:599–621.
18. Lee SC, Bankoff SG. Parametric effects on the onset of flooding in flat-plate geometries. *Int J Heat Mass Transf.* 1984;27:1691–1700.
19. Biage M, Delhaye JM, Vernier P. The flooding transition: a detailed experimental investigation of the liquid film before the flooding point. ANS Proceedings, National Heat Transfer Conference, Philadelphia, PA. ANS, 1989:53–60.
20. Zapke A, Kroeger DG. Counter-current gas-liquid flow in inclined and vertical ducts. I. Flow patterns, pressure drop characteristics and flooding. *Int J Multiphase Flow*. 2000;26:1439–1455.
21. Zapke A, Kroeger DG. Counter-current gas-liquid flow in inclined and vertical ducts. II. The validity of the Froude-Ohnesorge number correlation for flooding. *Int J Multiphase Flow*. 2000;26:1457–1468.
22. Vlachos NA, Paras SV, Mouza AA, Karabelas AJ. Visual observations of flooding in narrow rectangular channels. *Int J Multiphase Flow*. 2001;27:1415–1430.
23. Sudo Y. Mechanism and effects of predominant parameters regarding limitation of falling water in vertical counter-current two-phase flow. *J Heat Transf (Transactions of the ASME)*. 1996;118:715–724.
24. Hewitt GF. In search of two-phase flow. 30th US National Heat Transfer Conference, Portland, Oregon, 1995.
25. Demekhin EA, Tokarev GY, Shkadov VY. Instability and nonlinear waves for the vertical counter-current flow of a liquid film and turbulent gas. *Teoretichieskie Osnovy Khimicheskoi Tekhnologii.* 1989; 23:64–70.
26. Benjamin TB. Shearing flow over a wavy boundary. *J Fluid Mech.* 1959;6:161–205.
27. Miles JW. On the generation of surface waves by shear flows. *J Fluid Mech.* 1957;3:185–204.
28. Dietze GF, Leefken A, Kneer R. Investigation of the backflow phenomenon in falling liquid films. *J Fluid Mech.* 2008;595:435–459.
29. Trifonov YY. Wavy film flow down a vertical plate: comparisons between the integral approaches results and the full-scale computations. *J Eng Thermophys.* 2008;17:30–52.
30. Malamataris NA, Vlachogiannis M, Bontozoglou V. Solitary waves on inclined films: flow structure and binary interactions. *Phys Fluids*. 2002;14:1082–1094.
31. Schlichting H. *Boundary layer theory*. Moscow: Publishing House "Nauka", 1974.

Appendix A

Details of the governing equations transformation and the numerical algorithm

We consider the steady-state travelling solutions of the Eqs. 1–12. The coordinates transformation $x_1 = x - ct$, $\eta = y/H(x - ct)$, $\tilde{\eta} = (0.5 - \varepsilon_2 y)/(0.5 - \varepsilon_2 H)$ defines the flow area: $x_1 \in [0, 1]$, $\eta \in [0, 1]$, $\tilde{\eta} \in [0, 1]$ and allows us to write the governing equations as follows (further, we omit the subscript "1"):

$$c\frac{\partial u}{\partial x} + \eta_x c\frac{\partial u}{\partial \eta} - \frac{\partial \bar{P}}{\partial x} - \eta_x\frac{\partial \bar{P}}{\partial \eta} - Z\varepsilon_\rho n^2 + \frac{1}{\varepsilon \mathrm{Re}}\left[3 + \eta_y^2\frac{\partial^2 u}{\partial \eta^2} + \varepsilon^2\left(\frac{\partial^2 u}{\partial x^2} + \eta_x^2\frac{\partial^2 u}{\partial \eta^2} + 2\eta_x\frac{\partial^2 u}{\partial x \partial \eta} + (\eta_{x\xi} + \eta_x\eta_{x\eta})\frac{\partial u}{\partial \eta}\right)\right] - \eta_y\frac{\partial uv}{\partial \eta} - \frac{\partial u^2}{\partial x} - \eta_x\frac{\partial u^2}{\partial \eta} = 0; \quad \text{(A1)}$$

$$-\eta_y\frac{\partial \bar{P}}{\partial \eta} + \frac{\varepsilon}{\mathrm{Re}}\left[\eta_y^2\frac{\partial^2 v}{\partial \eta^2} + \varepsilon^2\left(\frac{\partial^2 v}{\partial x^2} + \eta_x^2\frac{\partial^2 v}{\partial \eta^2} + 2\eta_x\frac{\partial^2 v}{\partial x \partial \eta} + (\eta_{x\xi} + \eta_x\eta_{x\eta})\frac{\partial v}{\partial \eta}\right)\right] - \varepsilon^2\left(-c\frac{\partial v}{\partial x} - \eta_x c\frac{\partial v}{\partial \eta} + \frac{\partial uv}{\partial x} + \eta_x\frac{\partial uv}{\partial \eta} + \eta_y\frac{\partial v^2}{\partial \eta}\right) = 0; \quad \text{(A2)}$$

$$v(x,\eta) = -H(x)u(x,\eta)\eta_x - \frac{\partial}{\partial x}\left(H\int_0^\eta u(x,\eta')d\eta'\right); \quad \text{(A3)}$$

$$H(x)\int_0^1 (u(x,\eta') - c)d\eta' = 1 - c\langle H\rangle; \quad \text{(A4)}$$

$$u(x,\eta) = 0, \quad \eta = 0; \quad \text{(A5)}$$

$$\bar{P} - \varepsilon_\rho n^2 \bar{P}^g = \frac{2\varepsilon}{\mathrm{Re}}\left(\eta_y\frac{\partial v}{\partial \eta} - \varepsilon_\mu n\tilde{\eta}_y\frac{\partial v^g}{\partial \tilde{\eta}}\right)\frac{1 + \varepsilon^2\left(\frac{dH}{dx}\right)^2}{1 - \varepsilon^2\left(\frac{dH}{dx}\right)^2} - \varepsilon^2\frac{(3Fi)^{1/3}}{\mathrm{Re}^{5/3}}\frac{\frac{d^2H}{dx^2}}{\left[1 + \varepsilon^2\left(\frac{dH}{dx}\right)^2\right]^{3/2}}, \quad \eta = \tilde{\eta} = 1; \quad \text{(A6)}$$

$$\left[\eta_y\frac{\partial u}{\partial \eta} - \varepsilon_\mu n\tilde{\eta}_y\frac{\partial u^g}{\partial \tilde{\eta}} + \varepsilon^2\left(\frac{\partial v}{\partial x} - \varepsilon_\mu n\frac{\partial v^g}{\partial x}\right) + \varepsilon^2\left(\eta_x\frac{\partial v}{\partial \eta} - \varepsilon_\mu n\tilde{\eta}_x\frac{\partial v^g}{\partial \tilde{\eta}}\right)\right] \bullet \left[1 - \varepsilon^2\left(\frac{dH}{dx}\right)^2\right] + 4\varepsilon^2\left(\eta_y\frac{\partial v}{\partial \eta} - \varepsilon_\mu n\tilde{\eta}_y\frac{\partial v^g}{\partial \tilde{\eta}}\right)\frac{dH}{dx} = 0, \quad \eta = \tilde{\eta} = 1. \quad \text{(A7)}$$

$$u = nu^g, \ \eta = \tilde{\eta} = 1; \quad \text{(A8)}$$

$$v^g(x,\tilde{\eta}) = u^g(x,\tilde{\eta})\tilde{\eta}\frac{dH}{dx} + \frac{1}{\varepsilon_2}\frac{\partial}{\partial x}\left((0.5 - \varepsilon_2 H)\int_0^{\tilde{\eta}} u^g(x,\tilde{\eta}')d\tilde{\eta}'\right); \quad \text{(A9)}$$

$$(0.5 - \varepsilon_2 H)\int_0^1 \left(u^g(x,\tilde{\eta}') - \frac{c}{n}\right)d\tilde{\eta}' = -1 - \frac{c}{n}(0.5 - \varepsilon_2\langle H\rangle); \quad \text{(A10)}$$

$$\frac{c}{n}\frac{\partial u^g}{\partial x}+\tilde{\eta}_x\frac{c}{n}\frac{\partial u}{\partial\tilde{\eta}}-\frac{\partial\bar{P}^g}{\partial x}-Z-\tilde{\eta}_x\frac{\partial\bar{P}^g}{\partial\tilde{\eta}}+\frac{1}{\varepsilon\varepsilon_2\mathrm{Re}^g}\left[\tilde{\eta}_y^2\frac{\partial^2u^g}{\partial\tilde{\eta}^2}+\varepsilon^2\left(\frac{\partial^2u^g}{\partial x^2}+\tilde{\eta}_x^2\frac{\partial^2u^g}{\partial\tilde{\eta}^2}+2\tilde{\eta}_x\frac{\partial^2u^g}{\partial x\partial\tilde{\eta}}+(\tilde{\eta}_{x\xi}+\tilde{\eta}_x\tilde{\eta}_{x\eta})\frac{\partial u^g}{\partial\tilde{\eta}}\right)\right]-\tilde{\eta}_y\frac{\partial u^g v^g}{\partial\tilde{\eta}}-\frac{\partial(u^g)^2}{\partial x}-\tilde{\eta}_x\frac{\partial(u^g)^2}{\partial\tilde{\eta}}=0; \quad \text{(A11)}$$

$$-\tilde{\eta}_y\frac{\partial\bar{P}^g}{\partial\tilde{\eta}}+\frac{\varepsilon}{\varepsilon_2\mathrm{Re}^g}\left[\tilde{\eta}_y^2\frac{\partial^2v^g}{\partial\tilde{\eta}^2}+\varepsilon^2\left(\frac{\partial^2v^g}{\partial x^2}+\tilde{\eta}_x^2\frac{\partial^2v^g}{\partial\tilde{\eta}^2}+2\tilde{\eta}_x\frac{\partial^2v^g}{\partial x\partial\tilde{\eta}}+(\tilde{\eta}_{x\xi}+\tilde{\eta}_x\tilde{\eta}_{x\eta})\bullet\frac{\partial v^g}{\partial\tilde{\eta}}\right)\right]-\varepsilon^2\left(-\frac{c}{n}\frac{\partial v^g}{\partial x}-\tilde{\eta}_x\frac{c}{n}\frac{\partial v^g}{\partial\tilde{\eta}}+\frac{\partial u^g v^g}{\partial x}+\tilde{\eta}_x\frac{\partial u^g v^g}{\partial\tilde{\eta}}+\tilde{\eta}_y\frac{\partial(v^g)^2}{\partial\tilde{\eta}}\right)=0; \quad \text{(A12)}$$

$$\frac{\partial u^g}{\partial\tilde{\eta}}=0,\tilde{\eta}=0\tilde{\eta}=0. \quad \text{(A13)}$$

Here $\eta_y = 1/H$; $\eta_x = -\eta(dH/dx)/H$; $\eta_{x\eta} = -\eta_y dH/dx$; $\tilde{\eta}_y = -\varepsilon_2/(0.5-\varepsilon_2 H)$; $\tilde{\eta}_x = \tilde{\eta}\varepsilon_2(dH/dx)/(0.5-\varepsilon_2 H)$; $\tilde{\eta}_{x\eta} = \tilde{\eta}_x/\tilde{\eta}$; $\eta_{x\xi} = -\eta_y(\eta_x dH/dx + \eta d^2H/dx^2)$; $\tilde{\eta}_{x\xi} = -\tilde{\eta}_y(\tilde{\eta}_x dH/dx + \tilde{\eta} d^2H/dx^2)$; $\langle\ldots\rangle$ is the value averaged over a wavelength.

Functions H, u, v, $\bar{P}$, u^g, v^g, $\bar{P}^g$ are periodic over the coordinate x and they are unknowns. We use spectral method to obtain the solutions of Eqs A1–A13:

$$u(x,\eta)=\frac{1}{2}U_1(x)+\sum_{m=2}^{M}U_m(x)T_{m-1}(\eta_1),\eta_1=2\eta-1,$$

$$U_m(x)=U_m^0+\sum_{\substack{k=-N/2+1\\k\neq0}}^{N/2-1}U_m^k\exp(2\pi ikx),\qquad (U_m^{-k})^*=U_m^k,\ m=1,\ldots,M.$$

$$u^g(x,\tilde{\eta})=\frac{1}{2}(U^g)_1(x)+\sum_{m=2}^{M^g}(U^g)_m(x)T_{m-1}(\tilde{\eta}_1),\ \tilde{\eta}_1=2\tilde{\eta}-1$$

$$(U^g)_m(x)=(U^g)_m^0+\sum_{\substack{k=-N/2+1\\k\neq0}}^{N/2-1}(U^g)_m^k\exp(2\pi ikx),\qquad ((U^g)_m^{-k})^*=(U^g)_m^k.$$

$$H(x)=H^0+\sum_{\substack{k=-N/2+1\\k\neq0}}^{N/2-1}H^k\exp(2\pi ikx),(H^{-k})^*=H^k.$$

$$\bar{P}^g(x,\tilde{\eta})|_{\tilde{\eta}=1}=\sum_{\substack{k=-N/2+1\\k\neq0}}^{N/2-1}(\bar{P}^g)^k\exp(2\pi ikx),\qquad ((\bar{P}^g)^{-k})^*=(\bar{P}^g)^k,(\bar{P}^g)^0\equiv0.$$

Here T_m (η_1) are Chebyshev polynomials and the "star" superscript designates complex conjugation.

The numerical algorithm starts with the specification of the initial approximation for harmonics $U_m^k, H^k, (U^g)_m^k, (\bar{P}^g)^k$ and for the values of Z and $\boldsymbol{c}$. There is a symmetry in the equations with respect to the coordinate shift $x \to x + const$. The phase of one of the film thickness harmonics can be defined beforehand due to this symmetry (for example $Real(H^1) = 0$). The value of the phase velocity $\boldsymbol{c}$ will be unknown instead of $Real(H^1)$ and the value of Z will be uknown instead of $(\bar{P}^g)^0$ which is equal to zero.

At $(M + M^g + 2)(N - 1)$ known values of $U_m^k, (U^g)_m^k, (\bar{P}^g)^k, Z, c, H^k$, the velocity $v(x,\eta)$ is unambiguously regenerated from Eq A3; $\bar{P}(x,\eta)$, from Eqs A2 and A6; $v^g(x,\tilde{\eta})$, from Eq A9; $\bar{P}^g(x,\tilde{\eta})$, from equation (A12). Using the Newton's iterative method and the Eqs. (A1), (A4), (A11) and (A10) transformed into (k, m)-space, we improve the initial approximation of the unknowns $(U_m^k, H^k, (U^g)_m^k, (\bar{P}^g)^k, Z, c)$. We use the first order differential scheme to calculate the Jacoby matrix. Taking into account the boundary conditions (A5), (A7), (A8) and (A13) we have $(M + M^g + 6)(N - 1)$ nonlinear algebraic equations to obtain $(M + M^g + 2)(N - 1)$ unknown values. The basis functions in the spectral expansion do not satisfy the boundary conditions and that is why the number of unknowns is less than the number of equations. We discard $4(N-1)$ equations corresponding to the last two Chebyshev coefficients in the expansion of the Eqs. A1 and A11. The results will be correct at a good enough accuracy of approximation of the functions $u(x,\eta)-\left|U_m^{N/2-1}\right|/\sup\left|U_m^k\right| < 10^{-3}$ at any m, and $\left|U_M^k\right|/\sup\left|U_m^k\right| < 10^{-3}$ at any k, and $u^g(x,\tilde{\eta}) - \left|(U^g)_m^{N/2-1}\right|/\sup\left|(U^g)_m^k\right| < 10^{-3}$ at any m, and $\left|(U^g)_{M^g}^k\right|/\sup\left|U_m^k\right| < 10^{-3}$ at any k. During the calculations, the corresponding increasing N, M and M^g (we varied value of N from 8 to 256 and values of M, M^g from 5 to 50, depending on the parameters) maintained the indicated conditions.

There is a "basic" solution of Eqs. A1–A13 that corresponds to the wavyless regime of the liquid/gas flow:

$$u_b(x,\eta)=\alpha_1\eta^2+\beta_1\eta, v_b(x,\eta)=0,\ P_b(x,\eta)=\varepsilon_\rho n^2 Z_b x, u_b^g(x,\tilde{\eta})=\alpha\tilde{\eta}^2+C, v_b^g(x,\tilde{\eta})=0, P_b^g(x,\tilde{\eta})=Z_b x,\alpha_1=2n\alpha-\frac{6}{H_b}-\frac{3n}{0.5-\varepsilon_2 H_b},\beta_1=-\frac{2}{3}\alpha_1+\frac{2}{H_b},n\alpha=\frac{6/H_b+4n/(0.5-\varepsilon_2 H_b)}{8/3+2\varepsilon_\mu\varepsilon_2 H_b/(0.5-\varepsilon_2 H_b)},\ \mathrm{C}=-\frac{\alpha}{3}-\frac{1}{0.5-\varepsilon_2 H_b},\ Z_b=\frac{2\alpha\varepsilon_2}{\varepsilon\mathrm{Re}^g(0.5-\varepsilon_2 H_b)^2},(H_b^3-1)(0.5-\varepsilon_2 H_b)^2\times[0.5-\varepsilon_2 H_b(1-3\varepsilon_\mu/4)]=9\varepsilon_\mu\varepsilon_2 H_b(0.5-\varepsilon_2 H_b/3)\times[0.5-\varepsilon_2 H_b(1-2n/3\varepsilon_2)]/4. \quad \text{(A14)}$$

Appendix B

The Orr-Sommerfeld equation to calculate the gas reaction to the wavy liquid film

Substitution of Eqs. 18–20 into the governing Eqs. 13–17 yields

$$2\pi ik\varepsilon\varepsilon_2 \mathrm{Re}^g\left[\frac{d^2u_b^g}{dy^2}F^k + u_b^g\varepsilon^2(2\pi k)^2F^k - u_b^g\frac{d^2F^k}{dy^2}\right] = -\frac{d^4F^k}{dy^4} + 2\varepsilon^2(2\pi k)^2\frac{d^2F^k}{dy^2} - \varepsilon^4(2\pi k)^4F^k; \quad \text{(B1)}$$

$$\left.\frac{dF^k}{dy}\right|_{y=0} = \left.\frac{du_b^g}{dy}\right|_{y=0};\ F^k\big|_{y=0} = 0; \left.\frac{d^2F^k}{dy^2}\right|_{y=0.5/\varepsilon_2} = F^k\big|_{y=0.5/\varepsilon_2} = 0; \quad \text{(B2)}$$

$$P_g^k = u_b^g\frac{dF^k}{dy} - \frac{du_b^g}{dy}F^k - \frac{i}{2\pi k\varepsilon\varepsilon_2\mathrm{Re}^g}\left[-\frac{d^3F^k}{dy^3} + (2\pi k\varepsilon)^2\frac{dF^k}{dy}\right]; \quad \text{(B3)}$$

To find functions $F^k(y)$ we solve these equations numerically for $k = 1,2, \ldots N/2-1$ Method uses the Chebyshev-series to solve a two-point boundary problem (B1–B2). We consider two cases of the basic gas velocity profile:

$$\text{Laminar-} \qquad u_b^g = 12\left(\varepsilon_2^2y^2 - \varepsilon_2 y\right), \lambda^f = \frac{24}{\mathrm{Re}^g}; \quad \text{(B4)}$$

Turbulent -

$$u_b^g = \begin{cases} -\eta\sqrt{\lambda^f/2},\ \eta < 8.74^{7/6} \\ -8.74\eta^{1/7}\sqrt{\lambda^f/2}, \eta > 8.74^{7/6} \end{cases},$$

$$\lambda^f = \frac{0.3164}{(4\mathrm{Re}^g)^{1/4}};\ \eta \equiv \varepsilon_2 y\mathrm{Re}^g\sqrt{\lambda^f/2}. \quad \text{(B5)}$$

Here λ^f is the friction coefficient and we take into account that the hydraulic diameter of our duct is 2D. Equation B5 are the well-known velocity distribution for the turbulent flow $(u_b^g)^*/v_* = 8.74\left(y^*v_*/v_g\right)^{1/7}$, $v_* = \sqrt{\tau_g/\rho_g}$, $\eta \equiv y^*v_*/v_g$ and the Blasius formula for the friction coefficient (see Schlichting[31]). Both for the laminar and turbulent flows the dimensional pressure and the interfacial shear are as follows:

$$(P_b^g)^* \equiv \frac{\lambda^f}{2D}\frac{\rho_g U_{GS}^2}{2}x* = \frac{2\tau_g}{D}x*,\ \tau_g \equiv \mu_g\left.\frac{d(u_b^g)^*}{dy*}\right|_{y*=0} = \lambda^f\frac{\rho_g U_{GS}^2}{8}. \quad \text{(B6, B7)}$$

Dimensionless value of the basic pressure is $P_b^g = \frac{\lambda^f\varepsilon_2 x}{\varepsilon}$. Velocity profiles (B4) and (B5) agree both with the condition (B7) $\left.\frac{du_b^g}{dy}\right|_{y=0} = -0.5\lambda^f\varepsilon_2\mathrm{Re}^g$ and with the condition $\int_0^{0.5/\varepsilon_2} u_b^g dy = -1/\varepsilon_2$

Governing Eqs. A1–A5 describe the liquid film flow and we need to modify the interface boundary conditions (A6)-(A7) to take into account our simplification of the gas reaction calculation:

$$\bar{P} - \varepsilon_\rho n^2\hat{P}^g\big|_{y=0} = \frac{2\varepsilon}{\mathrm{Re}}\left(\eta_y\frac{\partial v}{\partial\eta} - \varepsilon_\mu n\left.\frac{\partial\hat{v}^g}{\partial y}\right|_{y=0}\right)\frac{1+\varepsilon^2\left(\frac{dH}{dx}\right)^2}{1-\varepsilon^2\left(\frac{dH}{dx}\right)^2} - \varepsilon^2\frac{(3Fi)^{1/3}}{\mathrm{Re}^{5/3}}\frac{\frac{d^2H}{dx^2}}{\left[1+\varepsilon^2\left(\frac{dH}{dx}\right)^2\right]^{3/2}}, \eta = 1; \quad \text{(B8)}$$

$$\left[\eta_y\frac{\partial u}{\partial\eta} - \varepsilon_\mu n\left(\frac{du_b^g}{dy} + \frac{d^2u_b^g}{dy^2}H\right)\right|_{y=0} + \varepsilon^2\left(\frac{\partial v}{\partial x} + \eta_x\frac{\partial v}{\partial\eta}\right)\Bigg]\left[1-\varepsilon^2\left(\frac{dH}{dx}\right)^2\right] + 4\varepsilon^2\left(\eta_y\frac{\partial v}{\partial\eta} - \varepsilon_\mu n\left.\frac{\partial\hat{v}^g}{\partial y}\right|_{y=0}\right)\frac{dH}{dx} = 0, \eta = 1. \quad \text{(B9)}$$

Equations 16, 18, B2, and B3 give

$$\left.\frac{\partial\hat{v}^g}{\partial y}\right|_{y=0} = \frac{dH}{dx}\left.\frac{du_b^g}{dy}\right|_{y=0};$$

$$\hat{P}^g\big|_{y=0} = -\sum_{k=-N/2+1}^{N/2-1}\frac{i}{2\pi k\varepsilon\varepsilon_2\mathrm{Re}^g}\left[-\left.\frac{d^3F^k}{dy^3}\right|_{y=0} + (2\pi k\varepsilon)^2\left.\frac{du_b^g}{dy}\right|_{y=0}\right]H^k\exp(2\pi ikx).$$

Manuscript received Apr. 19, 2009, and revision received Oct. 22, 2009.